

Growth of amorphous carbon: Low-energy molecular dynamics simulation of atomic bombardment

K. Kohary and S. Kugler

Department of Theoretical Physics, Budapest University of Technology and Economics, H-1521 Budapest, Hungary

(Received 14 November 2000; revised manuscript received 6 February 2001; published 19 April 2001)

The growth of amorphous carbon thin film on a [111] diamond surface has been studied by a tight-binding molecular dynamics technique. Six different three-dimensional networks were constructed with periodic boundary conditions in two dimensions. Time-dependent nonequilibrium growth was simulated and densities, radial distribution functions, coordination numbers, bond angle distributions, and ring statistics were analyzed.

DOI: 10.1103/PhysRevB.63.193404

PACS number(s): 61.43.Dq, 61.43.Bn

At the early stage of the structure investigations the amorphous carbon (*a*-C) was studied by diffraction techniques.^{1–6} The first experiment was carried out by a Japanese group on an evaporated *a*-C sample using electron diffraction.¹ They proposed a microcrystalline model of *a*-C structure, consisting of graphitelike and diamondlike regions. A diffraction study of a small volume of *a*-C material, which sample was prepared by a filtered vacuum-arc method, measured nearly 100% of the sp^3 atomic configuration.⁴ Another neutron diffraction study was employed on an anomalous *a*-C sample in order to decide whether the structure has temperature dependence or not.⁵ The sample contained mostly sp^2 atomic arrangements.

There is no experimental method for the determination of microscopic structures in three dimensions. Efforts to develop simulation techniques for analyzing atomic scale structures are therefore continually being made. Monte Carlo and molecular dynamics (MD) simulations need potentials that are often difficult to derive yet are essential to simulations. Basically two different interatomic potentials are usually applied. The first set contains classical empirical potentials. Although simulations based on these potentials achieved remarkable success,^{7–10} extension of the simulation method to quantum mechanics is important. Structural simulations were carried out using *ab initio* or modified Car-Parinello density functional theory (DFT) method for *a*-C.^{11–13} An alternative possibility is to find tight-binding (TB) models that could be applied to larger systems (a few hundred atoms) and could be less time consuming than DFT. In the last decade applications of different TB potentials were widespread in the MD study of covalent systems.^{14–17}

In the experiments amorphous carbon films are usually prepared by evaporation growth techniques. During the evaporation, carbon atoms directed towards the target. If they reach the surface they could (i) scatter backwards, (ii) penetrate under the surface atoms, (iii) start collision-cascade, or (iv) chemically bond on the surface producing the growth of amorphous carbon. The processes mentioned [(i)–(iv)] mainly depend on the conditions of the environment. The most important parameters are substrate temperature T_{sub} and the kinetic energies E_{beam} of bombarding carbon atoms. The diamondlike amorphous carbon is usually prepared at low pressure (10^{-5} mbar), with the substrate temperature lower than 100 °C. In the experiments, negative bias is usually applied to accelerate the carbon ions from the

plasma, causing an extreme increase of initial kinetic energy (usually around 300–500 eV from 5–10 eV). However, there are some neutral atoms that mainly contribute to the surface growth because their kinetic energy (1–10 eV) is too low to penetrate under the surface. The aim of this Brief Report is to describe in detail the low energy (1–5 eV) bombardment of the target surface. In this case the occurrence of processes (ii) and (iii) is highly negligible.

Molecular dynamics simulations were carried out to study the dynamics of the growth process. The tight-binding Hamiltonian of Xu, Wang, Chan, and Ho¹⁷ was used to calculate interatomic potential between carbon atoms. This realistic TB potential has already been used for preparation of amorphous carbon¹⁸ and successfully applied for preparation of fullerenes.¹⁹

Our simulation technique was the following. An ideal diamond film consisting of 120 atoms was employed to model the substrate. The rectangular simulation cell was open along the positive z axis ([111] direction in our case) and periodic boundary conditions were used in x and y directions. Atoms in the bottom substrate layer were fixed at their ideal lattice positions, whereas the rest of the 96 atoms in the uppermost substrate layers were allowed to move with full dynamics. To simulate the constant substrate temperature the kinetic energy of the moveable atoms in the substrate were rescaled in every time step. The velocity Verlet algorithm was used to determine the phase trajectories of the carbon atoms. The time step was chosen to be equal to 0.5 fs.

Before starting the deposition process the substrate was kept at a given temperature for 0.5 ps in order to make structural relaxation. The neutral bombarding atoms were randomly placed in x and y directions above the substrate as near as possible, but not closer to any other atom than the cutoff distance of the potential. The initial velocities of bombarding atoms were directed to the substrate. There is no thermal equilibrium so initial velocities were chosen using the $v = [(2E_{\text{beam}}/m)(1.2 - 0.4p)]^{1/2}$ simple relation, where p is a uniformly distributed random number between 0 and 1. Directions were determined by $\theta = 120^\circ + p \times 60^\circ$ and $\phi = p \times 360^\circ$, where θ and ϕ are the polar angles and p is again a random number. The frequency of the atomic injection was $f = 1/125 \text{ fs}^{-1}$ on average. This flux is orders of magnitude greater than the deposition rate usually applied in real experiments. We found however, that even at such a

high flux the overheating effect of the surface (see, e.g., Kaukonen and Nieminen⁹) can be negligible and the low-energy evaporation can be modeled. The lower substrate temperatures applied in our simulations result in faster energy dissipation, which compensates for the high deposition rate.

Six different structures were made: models constructed simulating 25 ps and 40 ps (denoted by L) injection times and with average kinetic energy $E_{\text{beam}}=1$ eV and 5 eV at $T_{\text{sub}}=100$ K substrate temperature ($e1T100$, $e5T100$, $e1T100L$, and $e5T100L$) and two other models by 25 ps injection, $E_{\text{beam}}=1$ and 5 eV energy with substrate temperature of 300 K ($e1T300$, $e5T300$). In all cases the structures were relaxed for 5 ps after the deposition. During this period the substrate was kept at a constant temperature while the deposited networks were cooling down. The temperature versus time relation of this non-equilibrium process is a near-exponential function. The best fit was done according to $T_{\text{film}}(t)=c+\exp(at+b)$ K. The constant $c=150$ K was chosen rather than 100 K, which has a false asymptotic behavior, but it gave better fit (anomalous relaxation). Fitting parameters for the $e1T100L$ model are $a=-0.000935$ fs⁻¹ and $b=6.86$ and $c=150$ K. The relaxation time is $\tau\approx 1$ ps. The final structures of larger models ($e1T100L$ and $e5T100L$) made by different bombarding energies consist of almost the same number of atoms (177 and 172), with thickness of 12.65 Å and 10.98 Å. Models $e1T100$, $e5T100$, $e1T300$, and $e5T300$ have 126–129 atoms. Typical central processing unit (CPU) times of simulations are about 50–70 days on DEC-Alpha workstations. A snapshot of a film ($e5T100L$) is shown in Fig. 1 after relaxation. The substrate at $T_{\text{sub}}=100$ K remained similar to crystal lattice, while atoms left their position and the topological order became broken during growth at $T_{\text{sub}}=300$ K.

The time dependence of bond length and bond angle deviations were also investigated. In crystals, bond lengths and bond angles have only thermal disorder components. Non-crystalline materials have an additional broadening contribution to the bond length and bond angle distribution resulting from static disorder. First we calculated the standard deviations $\sigma(t_k)$ at discreet t_k in the following way:

$$\sigma(t_k) = \sqrt{\frac{1}{N} \sum_j \left(d_j(t_k) - \frac{\sum_{i=1}^N d_i(t_k)}{N} \right)^2},$$

where N is the number of bonds and $d_i(t_k)$ is the i th bond distance. Values in the range $0.095 \text{ \AA} < \sigma_b < 0.11 \text{ \AA}$ were obtained for bond length deviations. (The index b is for bond length.) Similar calculations for bond angle deviations provided $\sigma_\theta(t_k)$ within an interval of 11.7° – 12.8° . The contribution to standard deviation of thermal fluctuation was also studied as a function of time using the following term:

$$\sigma^{\text{th}}(t_k) = \sqrt{\frac{1}{N} \sum_i [d_i(t_k) - \langle d_i \rangle]^2},$$

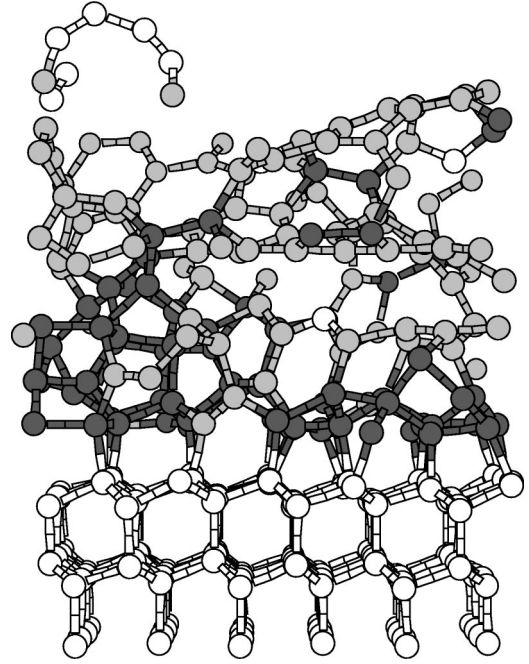


FIG. 1. A snapshot of the $e5T100L$ model is shown after growth and relaxation. The substrate (open circles at the bottom) at $T_{\text{sub}}=100$ K remained similar to the crystal lattice during growth. Black and gray atoms are fourfold and threefold coordinated, respectively. The rest of the open circles correspond to twofold- and one onefold-coordinated atoms. For a color version see <http://www.phy.bme.hu/~kohary/aCfigures.html>.

where time average $\langle d_i \rangle$ of bond d_i is used instead of $d_i(T=0)$.

As expected σ_b^{th} (and $\sigma_\theta^{\text{th}}$) versus time functions have an exponential decay as shown in Fig. 2. At the beginning of relaxation, when the temperature of the film is about 1000 K, the thermal part of the fluctuation is important ($\sigma_b \approx \sigma_b^{\text{th}}$, $\sigma_\theta \approx \sigma_\theta^{\text{th}}$). At the end it plays only a minor role ($\sigma_b \gg \sigma_b^{\text{th}}$, $\sigma_\theta \gg \sigma_\theta^{\text{th}}$). The σ_b^{th} (and $\sigma_\theta^{\text{th}}$) values as a function of temperature show linear relationships, as displayed in Fig. 3. The straight line does not intersect the origin because usually $\langle d_i \rangle \neq d_i(T=0)$.

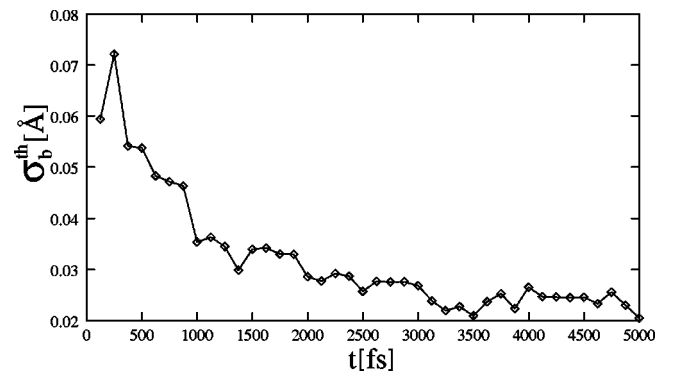


FIG. 2. As shown, expected σ_b^{th} vs time functions have an exponential decay. At the beginning of relaxation when the temperature of the film is about 1000 K the thermal part of the fluctuation is important while at the end it plays only a minor role.

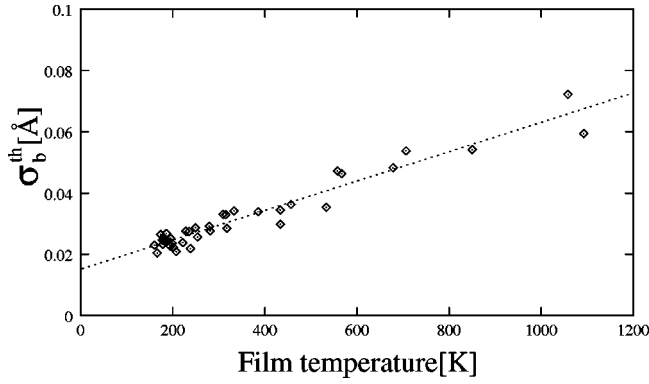


FIG. 3. σ_b^{th} in function of temperature shows a linear relationship. The straight line does not intersect the origin because usually $\langle d_i \rangle \neq d_i(T=0)$.

For density calculations, two different volumes were defined: we will refer to them as cells for the total sample and for the bulk. The bottom of the cells were 0.77 \AA lower than the bottom carbon atom in the amorphous network. This is almost at half bond distance between the upper substrate atoms and the bottom carbon atoms in the film. The top of the cells were determined differently. For the total sample the top of the cell was the highest z coordinate that occurs for atoms in the network. For the bulk z coordinate was less by 3 \AA . The x and y size of the cell was determined according to two-dimensional periodic boundary conditions. Table I contains the densities of different models. Each row is divided into two further rows. The upper rows constantly refer to the bulk and the lower rows refer to the total sample. For bulk models the densities are always larger than for the total sample. At $T_{\text{sub}}=100 \text{ K}$ bulk densities are between 2.7 and 3.0 g/cm^3 except model $e1T100L$, where the density is equal to 2.4 g/cm^3 . The reason for this lower density is that a void appeared at the top of the network, which drastically

TABLE I. It contains the number of atoms (No. C), the percentage of atoms with different coordination numbers (Z), the average coordination number $\langle Z \rangle$, the height z_d , and the density ρ . The two rows belong to bulk (top) and to the total (lower) sample, respectively. For bulk models the densities are always larger than for the total sample.

Model	No. C	$Z=2$	$Z=3$	$Z=4$	$\langle Z \rangle$	z_d (\AA)	ρ (g/cm^3)
$e1T100$	113	0.9	59.3	39.8	3.4	6.5	3.0
	129	7.0	56.6	34.9	3.2	9.5	2.3
$e5T100$	124	4.8	58.1	37.1	3.3	7.7	2.7
	129	7.0	55.8	35.7	3.3	10.7	2.0
$e1T300$	121	5.8	71.9	21.5	3.1	9.8	2.0
	130	7.7	70.8	20.0	3.1	12.8	1.6
$e5T300$	92	0.0	68.5	31.5	3.3	6.3	2.3
	126	11.1	64.3	24.6	3.1	9.3	2.1
$e1T100L$	160	5.0	65.0	30.0	3.2	11.0	2.4
	177	9.0	62.1	27.1	3.1	14.0	2.1
$e5T100L$	151	2.0	55.6	42.4	3.4	9.4	2.7
	172	4.7	56.4	38.4	3.3	12.4	2.3

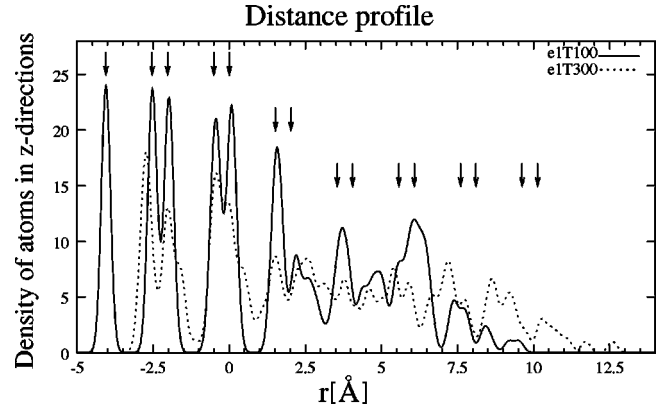


FIG. 4. Density profiles of two growth films, $e1T100$ (solid line) and $e1T300$ (dotted line), are displayed perpendicular to the substrate surface. Arrows represent the layer positions in a perfect diamond crystal. The difference in temperature between the two substrates causes a difference between memory effects.

decreased the local density. At $T_{\text{sub}}=300 \text{ K}$ the structures are less dense ($2.0\text{--}2.3 \text{ g/cm}^3$).

In Fig. 4 density profiles of two networks ($e1T100$ and $e1T300$) are displayed perpendicular to the substrate surface. The arrows represent the layer positions of a perfect diamond crystal. The difference in temperature between two substrates causes differences between memory effects. The structure on the surface at 100 K has a more pronounced layering effect than the other network on substrate at room temperature. In the first $3\text{--}4 \text{ \AA}$ thick layers over the $[111]$ surface the sp^3 content is high due to the memory effect. In the rest of the bulk the sp^2 content is dominant.

The two radial distribution functions (before and after relaxation) of any model are very similar, although peaks in the final structure seem to be a bit narrower and in the interval of $1.6\text{--}2.2 \text{ \AA}$ there are less bond lengths after relaxation. In Fig. 5 partial distribution functions $J_{i,j}$ of model $e1T100L$ can be seen, where i , and j denote the coordination numbers of the connected atoms. The average first-neighbor distances are 1.43 \AA , 1.52 \AA , and 1.59 \AA for $J_{3,3}$, $J_{3,4}$, and $J_{4,4}$, respectively.

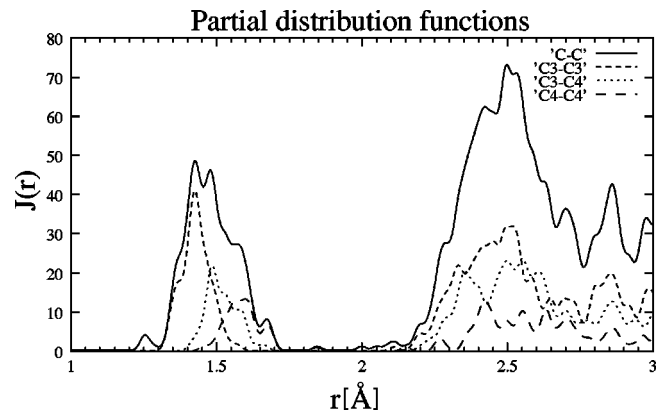


FIG. 5. Partial distribution functions $J_{i,j}$ can be seen where i,j note the coordination numbers of the connected atoms. $J_{3,3}$, $J_{3,4}$, and $J_{4,4}$ peaks are shown. The average bond distances are 1.43 \AA , 1.52 \AA , and 1.59 \AA , respectively.

For bond counting we used a value of 1.85 Å as an upper limit of bond length inside the first coordination shell. Table I shows the percentage of different coordinations. There is no five- or sixfold atom. More than half of the atoms have the sp^2 bonding configuration in the models, as shown in Table I. The average coordination numbers in the bulk were slightly over the graphite coordination. The dominating part of fourfold-coordinated atoms is near the substrate and the contribution to twofold-coordinated atoms is due to the atoms at the top of the amorphous network (see Fig. 1). The *e5T100L* model contains a onefold-coordinated carbon atom at the end of a chain. When comparing the average coordination numbers it is evident that there are no drastic differences among the models simulated. An MD simulation of Kaukonen and Nieminen,⁹ using the classical empirical potential of Tersoff, shows that the same portion of sp^2 but the $sp^2:sp^3$ ratio is slightly different at $T_{\text{sub}}=300$ K. At the $E_{\text{beam}}=1$ eV beam energy 5.8:71.9:21.5 is the ratio in the *e1T300* model, while it is 19.0:73.2:6.7 in their case. Our sample has a higher portion of diamondlike atoms and less twofold-coordinated carbon atoms at the same conditions.

Angles can be analyzed in detail according to the coordination numbers of the neighbors and the center (e.g., C3-C4-C3, C4-C4-C4, etc.). Atoms with sp^3 local arrangements have nearly the same average values in the C3-C4-C3, C3-C4-C4, and C4-C4-C4 cases, which are around the tetrahedral angle. Clear differences are observed for sp^2 configurations. C4-C3-C4 angles have much less average values than the others. The latter average bond angles are close to 120°. It means that threefold-coordinated central atoms with at least two C3 first neighbors are always near planar structures even if the third one is C4.

The ring statistics for our models were also calculated. A fourfold ring was found in the sample made with

$E_{\text{beam}}=1$ eV at $T_{\text{sub}}=100$ K substrate temperature but there was no threefold ring in our simulation. In the graphitic and diamond network, sixfold, eightfold, etc., coordinations are present. In our models even-numbered as well as odd-membered rings can be found. It seems clear that lower beam energy shows less 4–7-membered rings than higher bombarding energy.

In summary, low-energy molecular dynamics simulations of atomic beam growth on a diamond [111] surface were carried out using two different average carbon beam energies, $E_{\text{beam}}=1$ and 5 eV and two different substrate temperatures, $T_{\text{sub}}=100$ and 300 K. Six networks were prepared by atom deposition with periodic boundary conditions in two dimensions and the most important structural parameters were compared. Our aim was to construct large-scale amorphous carbon models of over 100 atoms by using quantum-mechanical treatment. The atomic interactions were calculated by a well-tested tight-binding potential. The growing process was described as in real experiments without any artificial model of energy dissipation;^{9,20} however, the deposition rate was much higher than is usually applied in experiments. Other studies on the growth process use similar rates. On the basis of our time-dependent investigation we expect that much lower deposit rates do not cause a significant difference in our models. The influence of our lower substrate temperature is that the energy dissipation is faster and this slightly compensates for the high deposition rate. Unfortunately, it is clear that real experimental rates cannot be implemented for computer simulation in the near future.

This work has been supported by the Fund OTKA (Grant No. T029813, T032193, T033004). One of the authors (K. Kohary) would like to thank Professor Th. Frauenheim and Professor P. Thomas who provided him with use of the computer facilities in Paderborn and Marburg.

-
- ¹J. Kakinoki, K. Katada, T. Hanawa, and T. Ino, *Acta Crystallogr.* **13**, 171 (1960).
²D.F.R. Mildner and J.M. Carpenter, *J. Non-Cryst. Solids* **47**, 381 (1982).
³F. Li and J.S. Lannin, *Phys. Rev. Lett.* **65**, 1905 (1990).
⁴P.H. Gaskell, A. Saeed, P. Chieux, and D.R. McKenzie, *Phys. Rev. Lett.* **67**, 1286 (1991).
⁵S. Kugler, K. Shimakawa, T. Watanabe, K. Hayashi, I. László, and R. Bellissent, *J. Non-Cryst. Solids* **164-166**, 831 (1993).
⁶K.W.R. Gilkes, P.H. Gaskell, and J. Robertson, *Phys. Rev. B* **51**, 12 303 (1995).
⁷J. Tersoff, *Phys. Rev. Lett.* **61**, 2879 (1988).
⁸D.W. Brenner, *Phys. Rev. B* **42**, 9458 (1990).
⁹H.-P. Kaukonen and R.M. Nieminen, *Phys. Rev. Lett.* **68**, 620 (1992).
¹⁰P.C. Kelires, *Phys. Rev. B* **47**, 1829 (1993).
¹¹G. Galli, R.M. Martin, R. Car, M. Parrinello, *Phys. Rev. Lett.* **62**, 555 (1989).
¹²N.A. Marks, D.R. McKenzie, B.A. Pailthorpe, M. Bernasconi, and M. Parriello, *Phys. Rev. B* **54**, 9703 (1996).
¹³D.G. McCulloch, D.R. McKenzie, and C.M. Goringe, *Phys. Rev. B* **61**, 2349 (2000).
¹⁴D. Porezag, Th. Frauenheim, Th. Koehler, G. Seifert, and R. Kaschner, *Phys. Rev. B* **51**, 12 947 (1995).
¹⁵D.A. Drabold, P.A. Fedders, and P. Stumm, *Phys. Rev. B* **49**, 16 415 (1994).
¹⁶Th. Köhler, Th. Frauenheim, and G. Jungnickel, *Phys. Rev. B* **52**, 11 837 (1995).
¹⁷C.H. Xu, C.Z. Wang, C.T. Chan, and K.M. Ho, *J. Phys.: Condens. Matter* **4**, 6047 (1992).
¹⁸C.Z. Wang, K.M. Ho, and C.T. Chan, *Phys. Rev. Lett.* **70**, 611 (1993).
¹⁹I. László, *Europhys. Lett.* **44**, 741 (1998); I. László, *J. Mol. Struct.: THEOCHEM* **463**, 181 (1999).
²⁰K. Kohary and S. Kugler, *J. Non-Cryst. Solids* **266-269**, 746 (2000).